Supplementary Information for:

PVA reinforced gossypolone and doxorubicin π–π stacking nanoparticles towards tumor targeting and ultralow dose synergistic chemotherapy

Yiming Liu,[a] Ke Li,[b] Youshen Wu,[c] Jingwen Ma,[a] Peng Tang,[a] Yongchun Liu[a] and Daocheng Wu*[a]

[a] *Key Laboratory of Biomedical Information Engineering of Education Ministry, School of Life Science and Technology, Xi'an Jiaotong University, Xi'an 710049, China.*

[b] *Shaanxi Key Laboratory of Ischemic Cardiovascular Disease, Institute of Basic and Translational Medicine, Xi'an Medical University, Xi'an 710021, China.*

[c] *Department of Chemistry, School of Science, Xi'an Jiaotong University, Xi'an 710049, PR China*

Experimental

Toxicity of HA-Gn@DPGn NPs

Male BALB/c mice (n = 10) were adapted to the condition 3 days before injecting drugs. The mice were randomly distributed into 2 groups: (1) HA-Gn and (2) PBS. The body weight was measured every other day. The survival rates were calculated via counting the number of deaths 14 days after injection.

For blood hemolysis, red blood cells were collected from the whole blood of mice after centrifugation, and were washed with PBS for 5 times. Red blood cells were resuspended in different solutions (1 mL). PBS and water were used as negative control and positive control, respectively. HA-Gn solutions at different concentrations and control groups were incubated at 37 °C. After 2h, these results were recorded by UV-Vis at 541 nm. The hemolysis rate (%) was calculated as follows:

$$\text{Hemolysis}\,(\%) = \frac{A - A_n}{A_p - A_n} \times 100\%$$

where A is the absorbance of samples, A_n is the absorbance of negative control, and A_p is the absorbance of positive control.

Intratumoral inhibition efficacy

When the tumors grew to an appropriate size (~100 mm^3), the mice were randomly assigned into 4 groups : (1) PBS (control), (2) free Gn (1.5 mg/kg), (3) free DOX (0.03 mg/kg), and (4) free Gn (1.5 mg/kg) and DOX (0.03 mg/kg). Due to the specificity of intratumoral administration (tumor damage), we choose to intratumoral injection once. Tumor size and body weight were measured to assess tumor growth inhibition after injection. At 10th days, all mice were sacrificed via CO_2 overdose.

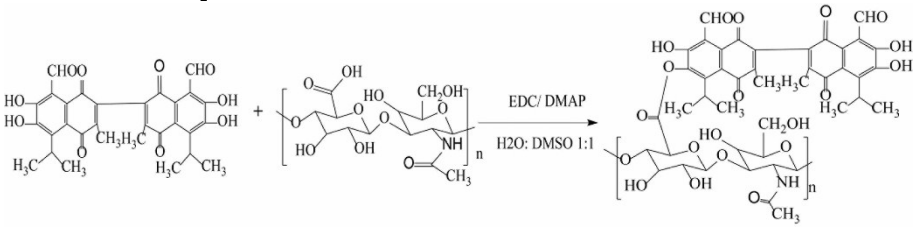

Scheme S1 Chemical equation of HA-Gn synthesis.

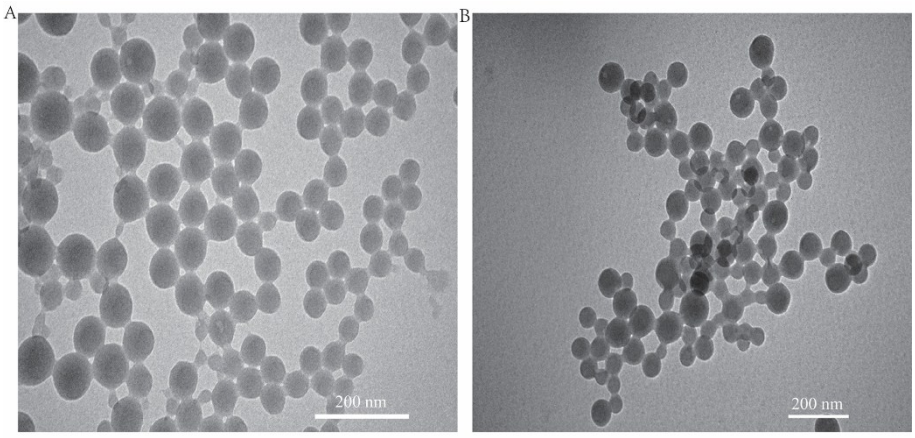

Fig. S1 TEM images of Gn NPs and DGn NPs.

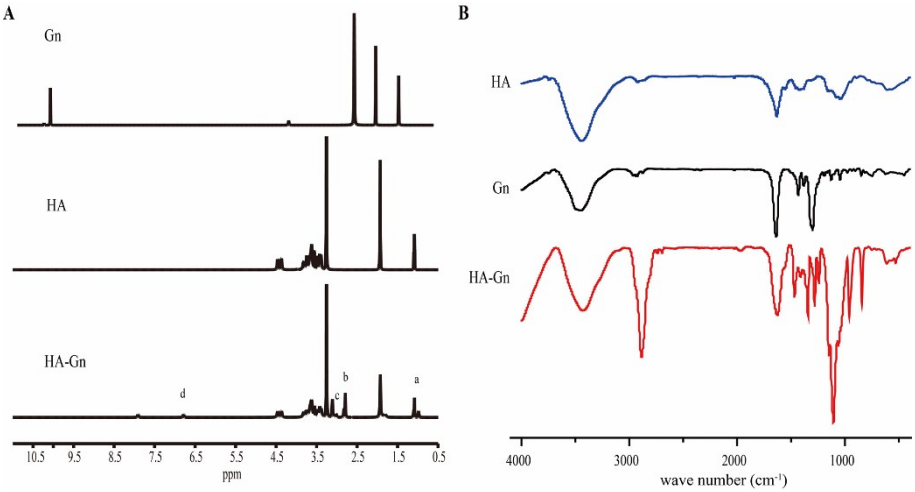

Fig. S2 Chemical structure of HA-Gn.

The chemical structure of HA-Gn was confirmed by FTIR and ^{1}H NMR. Fig. S1 B shows the FTIR spectra of HA, Gn and HA-Gn. The FTIR absorption spectra of HA-Gn showed new peaks at 1468 cm^{-1} ($\nu_{C=O}$, ester) and 1282 cm^{-1} (ν_{C-O-C}, ester), which indicated newly formed ester bonds (COO–). This finding proved that new of modified compounds HA-Gn were synthesized by forming ester bond among HA and Gn. Moreover, ^{1}H NMR was used to confirm that Gn was introduced into HA, as shown in Fig. S1 A. The ^{1}H NMR spectra of HA-Gn showed additional peaks compared with HA. Detailed analysis of ^{1}H NMR is as follows: δ = 0.99 ppm and δ = 1.82 ppm (a) characterized the H in –CH of isopropyl; δ = 2.79 ppm and δ = 3.11 ppm (b) characterized the H in –CH_3 of isopropyl; δ = 3.02 ppm and δ = 3.06 ppm (c) characterized H in –CH_3 of the naphthalene ring; δ = 6.79 and δ = 7.91 ppm (d) characterized H in –CHO. The differences between the chemical shifts of peaks HA-Gn and Gn were mainly caused by the variation of chemical environment of hydrogen atoms. Therefore, all the mentioned above facts demonstrated that the HA modifier HA-Gn were produced through condensation reaction between the carboxyl acid of HA and the hydroxyl on Gn. The substitution values of HA were 7.8 ± 1.6 %.

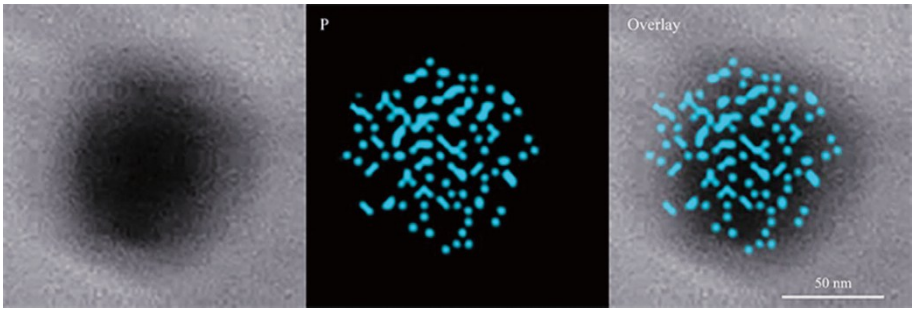

Fig. S3 TEM image of HA-Gn@DPGn NPs and elements mapping.

As a derivative of PVA, ammonium alcohol polyvinyl phosphate was used to substitute PVA to obtain the

distribution of PVA in HA-Gn@DPGn NPs by element mapping.

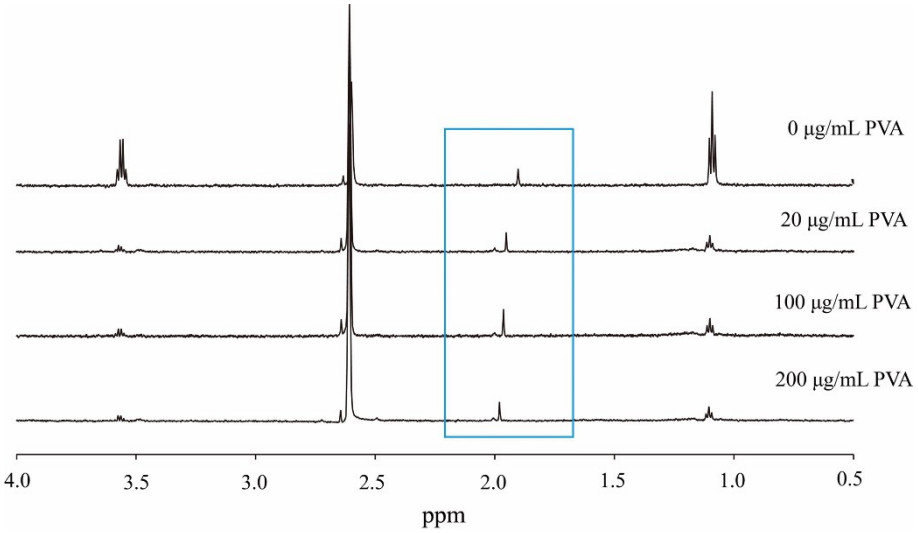

Fig. S4 The NMR spectra of DPGn NPs with different concentration PVA.

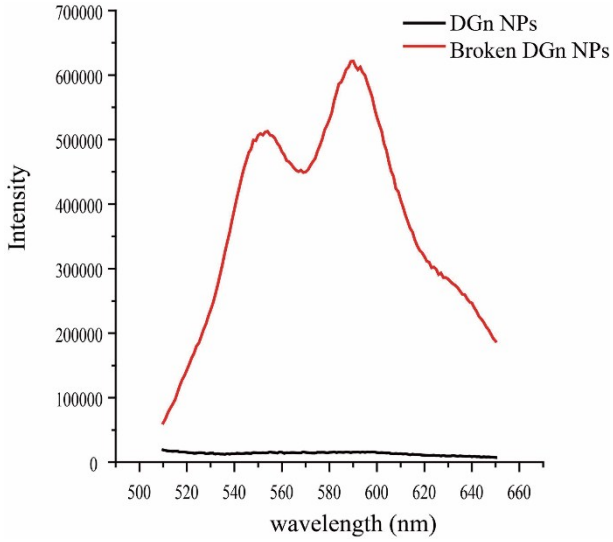

Fig. S5 The fluorescence of DOX varying the formation of DGn NPs.

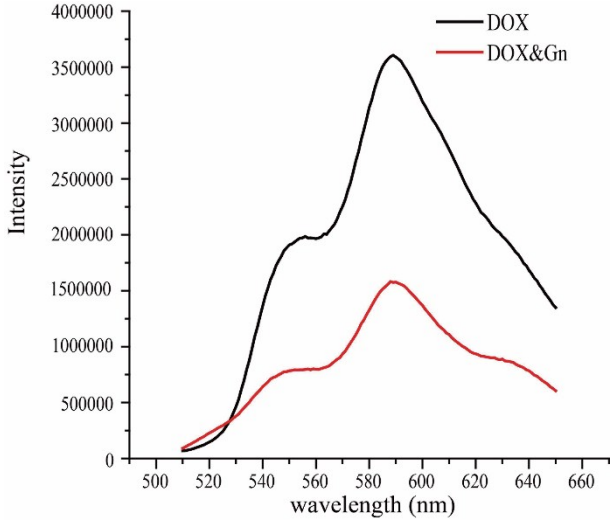

Fig. S6 The fluorescence of DOX after the addition of Gn.

As shown in Fig. S5, the fluorescence of DOX was qunenched when Gn and DOX aggregated together through π–π stacking. After DGn NPs were broken, the fluorescence appeared again. Obviously, free DOX had very strong fluorescence intensity, which was higher than the intensity of free Gn-DOX mixture 2 fold (Fig. S6). These results

demonstrated that free Gn-DOX would qunench the fluorecence of DOX particially, on the contrast, DGn NPs would qunench the fluorence greatly. This phenomenon might caused by the short distence of molecules in nanoparticles. Thus, the change of fluorescence could be applied as the criterion for the formation of nanoparticles by Gn and othe fluorescent materials.

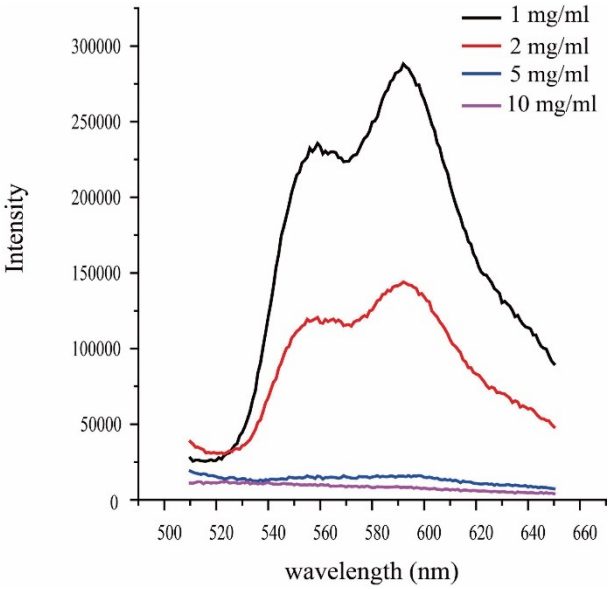

Fig. S7 The fluorescence of DOX at different Gn concentration in DGn NPs.

DGn NPs showed weak fluorescence intensity, though it was almost nonexistent compared to the intensity of the DOX. The fluorescence intensity of DGn NPs increased with the ratio of DOX:Gn increased. This finding was consistent with the previous results. Gn quenched the fluorescence after formed nanoparticles with fluorescent materials, which might be applied for further study.

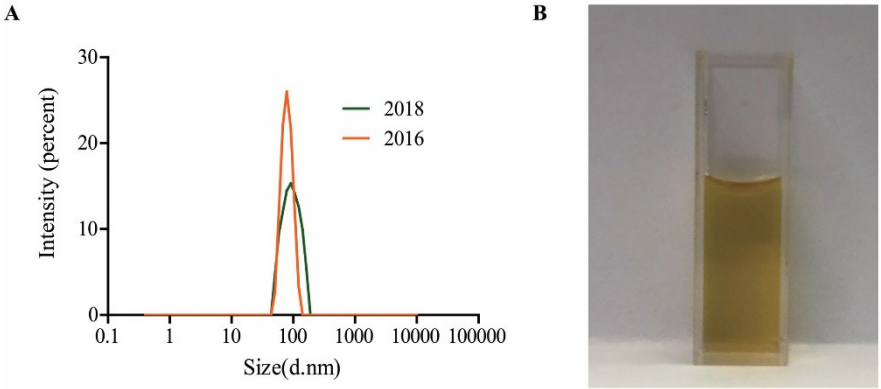

Fig. S8 (A) The DLS size profiles of HA-Gn@DPGn NPs freshly prepared (2016) and stored for 2 years (2018); (B) photographs of HA-Gn@DPGn NPs stored for 2 years.

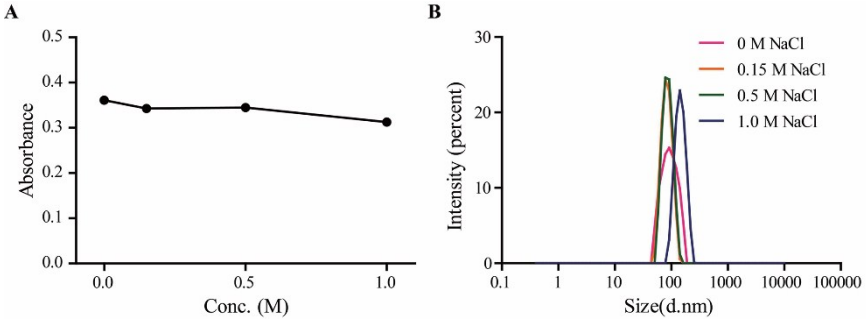

Fig. S9 (A) Turbidity of HA-Gn@DPGn NPs at different salt concentration; (B) DLS size profiles of HA-Gn@DPGn NPs NPs in aqueous solutions containing NaCl.

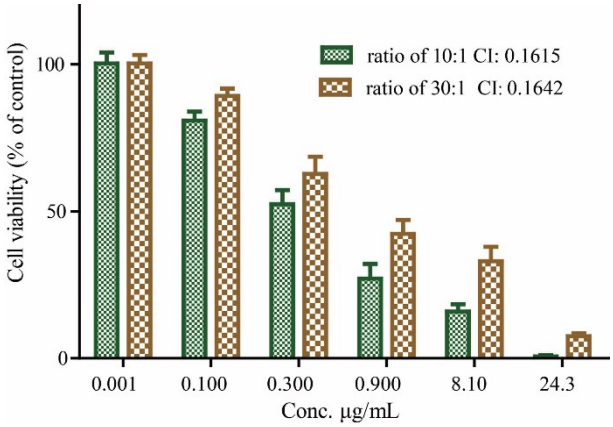

Fig. S10 Cell viability of Cl-1 cells treated with HA-Gn@DPGn NPs in different proportion.

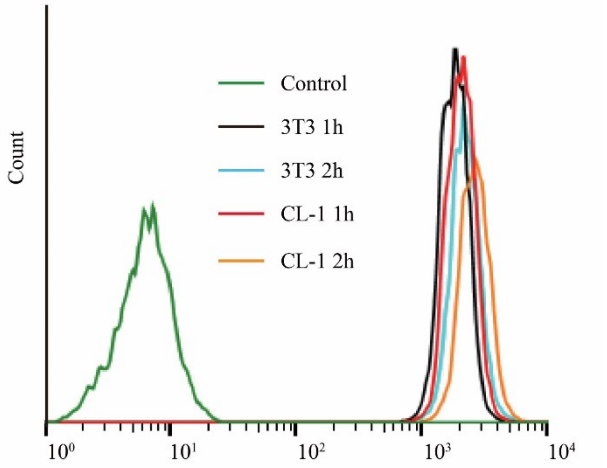

Fig. S11 Flow cytometry analysis of CL-1 cells and 3T3 cells were treated with free coumarin-6 at different time.

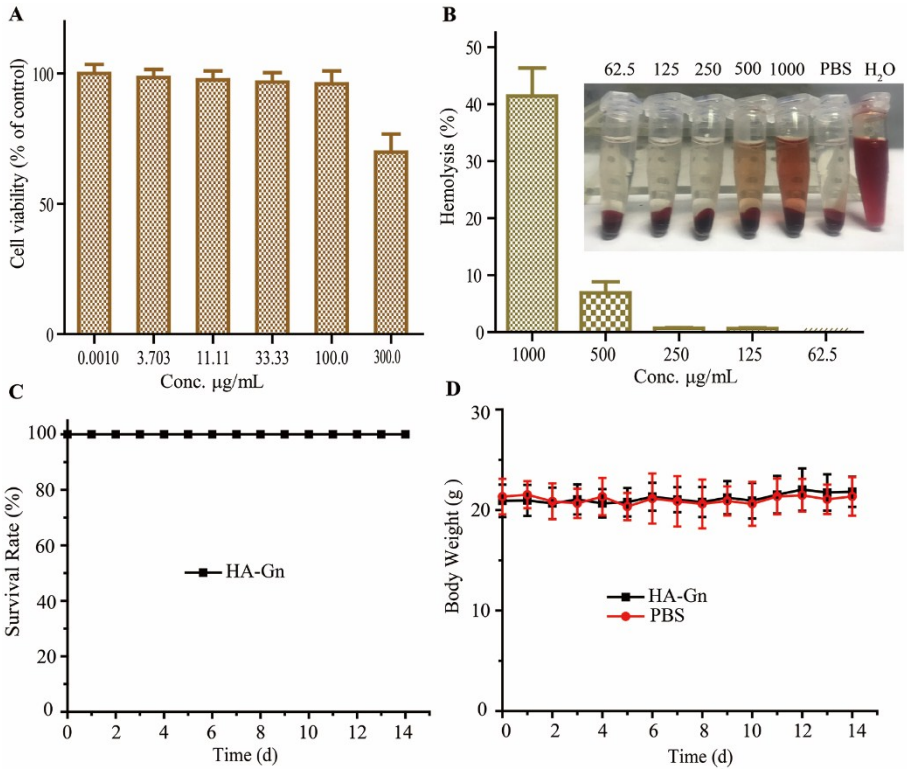

Fig. S12 The toxicity of HA-Gn. (A) Cell viability of Cl-1 cells treated with HA-Gn (n = 6). (B) Blood hemolysis test of HA-Gn at different concentrations (n = 3). (C) Survival Rate of HA-Gn (n = 10). (D) Body Weight.

HA-Gn had shown no significant cytotoxicity in the range of 100 μg/mL (Fig. S12A), but been toxic to cells at 300 μg/mL because of the instability ester bond, which caused cytotoxicity through the release of Gn from HA-Gn. Blood hemolysis test of HA-Gn showed similar results (Fig. S12B), 1000 μg/mL HA-Gn had a moderate hemolytic effect (< 50%) at 37 °C for 2h. These results improved a high biocompatibility of HA-Gn. Therefore, HA-Gn@DPGn NPs presented low toxicity and tumor targeting.

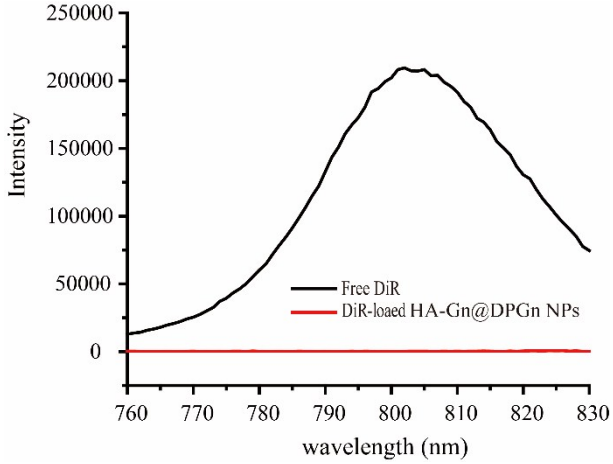

Fig. S13 The fluorescence of DiR varying the formation of free DiR and DiR loaded HA-Gn@DPGn NPs.

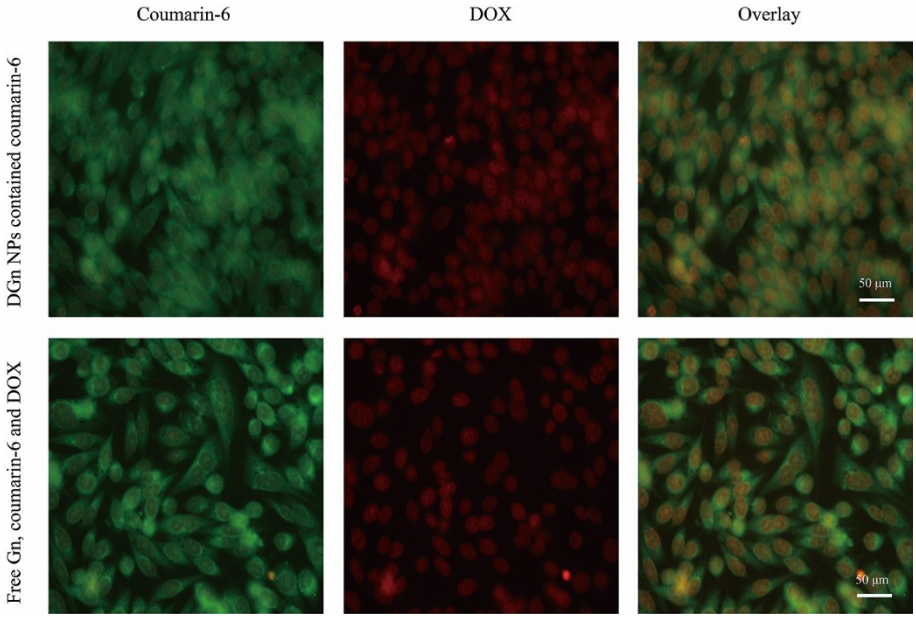

Fig. S14 Fluorescence images of PC-3 and cellular uptake behavior of DGn NPs containing coumarin-6 and the mixture of free Gn, coumarin-6 and DOX after 2h.

Fig. S14 showed the fluorescence imaging results of simple double-drug self-assembled aggregates DGn NPs. At 2h, DGn NPs exhibited same behaviors to the mixture of free Gn, coumarin-6 and DOX. These result proved DGn NPs were unstable under physiological condition.

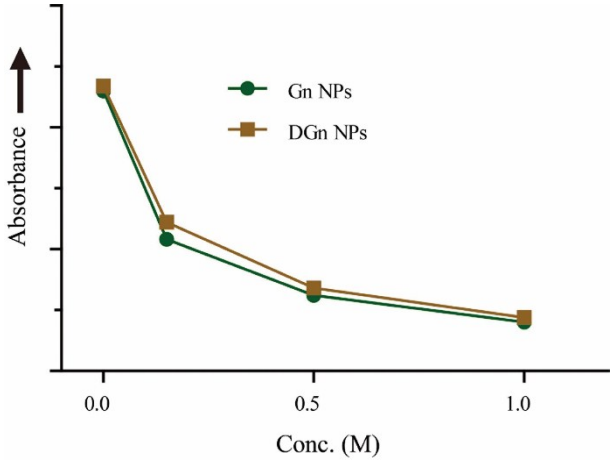

Fig. S15 Turbidity of Gn NPs and DGn NPs at different salt concentration

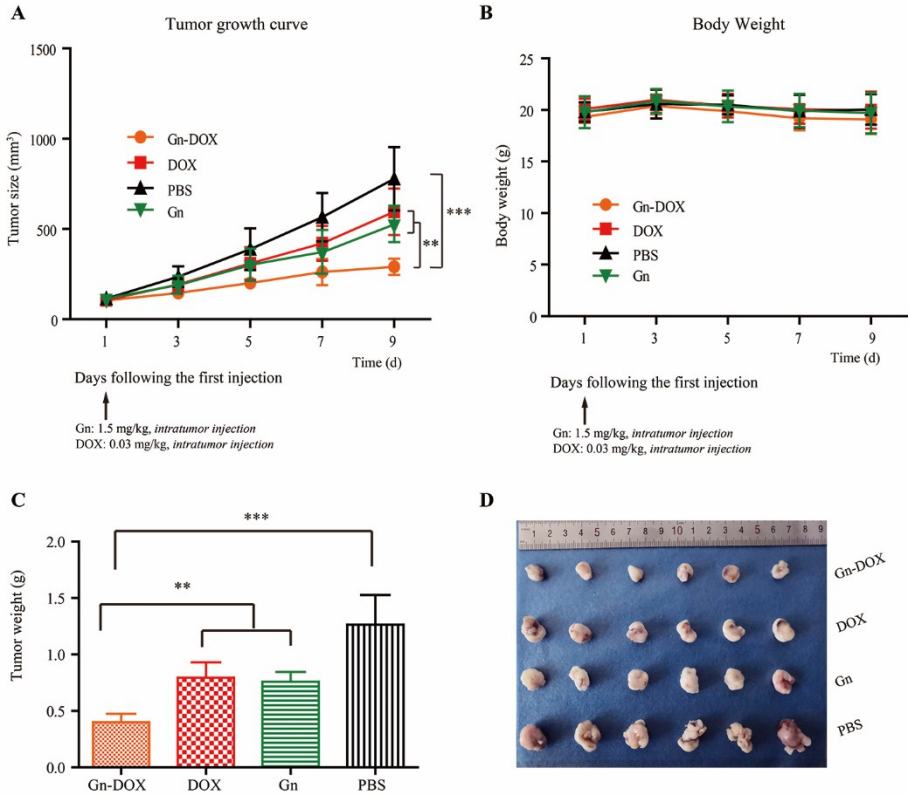

Fig. S16 (A) Tumor growth curves of mice treated with various formulas (n = 6). (B) The body weight change. (C) Average weights of tumors. (D) Photo of the excised tumors.

As shown in Fig. S16, free Gn-DOX group presented noticeable antitumor effects compared with other groups owing to significant synergism. This result is consistent with our conclusion that the combination of ultra-low dose DOX and Gn can produce a superior synergistic effect to chemotherapy.

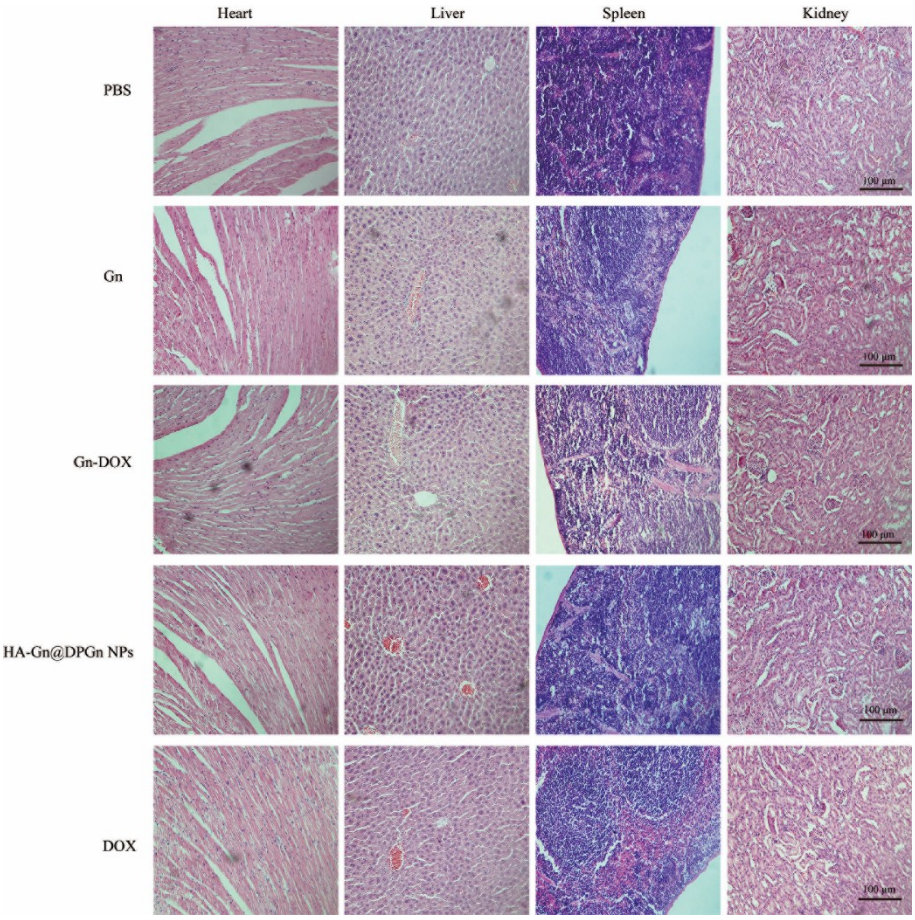

Fig. S17 HE staining of liver and heart tissues from different treatment groups.